

ORIGINAL RESEARCH ARTICLE

Machine learning-driven prediction of gel fraction in conductive gelatin methacryloyl hydrogels

Xi Huang*^{ORCID}, Ye Xuan Wong, Guo Liang Goh^{ORCID}, Xinchao Gao^{ORCID}, Jia Min Lee^{ORCID}, and Wai Yee Yeong*

School of Mechanical and Aerospace Engineering, Nanyang Technological University, Singapore

Abstract

Gelatin methacryloyl (GelMA) hydrogels, combined with conductive fillers like Poly(3,4-ethylenedioxythiophene) polystyrene sulfonate (PEDOT:SPSS), present significant promise for tissue regeneration due to their biocompatibility, biodegradability, and electrical conductivity. However, optimizing the curing process of the hydrogel is challenging due to a lack of an existing model for gel fraction prediction. This complexity is further heightened when additional variables such as bioink formulation and crosslinking parameters are considered. This study leverages machine learning (ML) to predict the gel fraction of GelMA-PEDOT:SPSS hydrogel based on the combination of three types of features: Bioink formulation, crosslinking parameters, and absorption coefficient. The two key objectives of this study are to develop an ML model to predict gel fraction from bioink formulation and crosslinking parameters such as ultraviolet (UV) power intensity and UV irradiation duration, and to create an ML model to predict gel fraction through the absorption coefficient instead of crosslinking parameter. In the first ML model, support vector regression achieved the highest accuracy with a mean absolute percentage error (MAPE) of 3.13% and an R^2 of 0.79. This model allows the user to select optimum bioink formulation and crosslinking parameters to achieve the required gel fraction with minimal experiment. For the second ML model that utilizes a combination of absorption coefficient and bioink formulation, deep neural network models achieved a MAPE of 6.31% and an R^2 of 0.54. The absorption coefficient model shows promise for a non-destructive, real-time assessment of gel fraction, enabling more precise control over the hydrogel properties during the curing process. These results demonstrate ML's capability to efficiently optimize hydrogel formulations, significantly cut down experimental efforts, and improve precision in 3D bioprinting and other hydrogel applications, thereby advancing the field of tissue regeneration.

*Corresponding authors:

Xi Huang
(huang.xi@ntu.edu.sg)
Wai Yee Yeong
(wyyeong@ntu.edu.sg)

Citation: Huang X, Wong YX, Goh GL, Gao X, Lee JM, Yeong WY. Machine learning-driven prediction of gel fraction in conductive gelatin methacryloyl hydrogels. *Int J AI Mater Design*. 2024;1(2):61-75.
doi: 10.36922/ijamd.3807

Received: May 31, 2024

Accepted: July 12, 2024

Published Online: August 8, 2024

Copyright: © 2024 Author(s). This is an Open-Access article distributed under the terms of the Creative Commons Attribution License, permitting distribution, and reproduction in any medium, provided the original work is properly cited.

Publisher's Note: AccScience Publishing remains neutral with regard to jurisdictional claims in published maps and institutional affiliations.

Keywords: 3D bioprinting; 3D printing; Biofabrication; Machine learning; Hydrogel; Composite

1. Introduction

Hydrogels have wide usage in 3D bioprinting application.¹⁻³ Among these, gelatin methacryloyl (GelMA) was highly valued due to its biocompatibility, biodegradability,

and tunable mechanical properties.^{4,5} These characteristics make GelMA an excellent candidate for creating extracellular matrix in the field of tissue regeneration. Electrical signals are crucial to the electroactive tissue in the human body, such as heart,⁶ muscles^{7,8} and nerves.⁹ The cells are highly regulated by affecting the intracellular signaling pathways as well as intracellular microenvironment.¹⁰ Therefore, the use of conductive hydrogel for tissue regeneration will facilitate the transmission of electrical signals, thereby promoting cell communication, proliferation, and differentiation within the engineered tissue.^{11,12} Poly(3,4-ethylenedioxythiophene) polystyrene sulfonate (PEDOT:SPSS) is known for its biocompatibility, solubility, excellent electrical conductivity, and mechanical flexibility.¹³⁻¹⁵ The integration of GelMA with PEDOT:SPSS opens up new avenues for developing multifunctional biomaterials that leverage the strengths of both components.^{16,17}

Adding conductive fillers such as PEDOT:SPSS into GelMA hydrogels significantly affects the curing process.^{18,19} The incorporation of these fillers can enhance the electrical conductivity of the hydrogel, which is beneficial for applications involving electroactive tissues.^{20,21} However, this enhancement comes with a tradeoff. The presence of conductive fillers can impede light transmission through the hydrogel, affecting how far the light can penetrate.^{16,22} Since the curing process of GelMA often relies on photoinitiated crosslinking, reduced light penetration can lead to incomplete or inefficient curing, compromising the mechanical properties and functionality of the hydrogel. The balance between conductive filler concentration and curing effectiveness is complex and requires careful optimization. Increasing the amount of conductive filler not only improves electrical conductivity but also decreases light transmission, necessitating a precise balance to achieve optimal curing efficiency. This delicate interplay between filler concentration and curing efficacy underscores the need for a comprehensive understanding of the curing dynamics and the material properties influenced by different filler concentrations.

Conventionally, the optimization for the crosslinking of hydrogel is done by performing experiments on a wide range of parameters, which is costly in terms of the materials used and time-consuming. The experimentation cost can be reduced by having a model to predict the gel fraction beforehand, while the precision of the crosslinking process can be improved with *in situ* characterization technique by fine-tuning the curing process in real time.²³⁻²⁵ There is an attempt on quantifying the degree of conversion (DoC) of photopolymerizing resin from the *in situ* measurement of the sample's refractive index,²⁴ but a bulky setup for the microscope system is required. For vat polymerization, *in situ* ultrasonic monitoring can help

in determining the DoC of the sample,²⁵ but may disrupt the cells in bioprinting. Most of the *in situ* measurement setup is too bulky to be integrated in a 3D printer or could be destructive to the bio-sample. Besides, although these methods can help with the *in situ* measurement of the crosslinking process, no prior work has been done on gel fraction prediction from the bioink formulation and crosslinking parameters to estimate the gel fraction before the experiment. There is a need for a model capable of predicting gel fraction based on the parameters before the experiment, and a model for an easier *in situ* measurement of the gel fraction.

Prediction and control of the gel fraction are of critical importance in tissue regeneration, particularly following the fabrication of engineered tissues and their subsequent transplantation into *in vivo* environments. The crosslinking parameters, including ultraviolet (UV) light power and exposure duration, significantly influence the gel fraction of the crosslinked hydrogel. On the one hand, if the engineered tissue is not fully cured, it will degrade more rapidly than anticipated. On the other hand, if the engineered tissues are overcured, there will be a dimensional mismatch between the designed structure and the actual tissue, which is especially problematic for certain structural features, such as narrowed channels within the engineered scaffold. This dimensional mismatch could impede the migration of cells into these channels, thereby hindering the tissue regeneration process.²⁶ While increasing the UV energy absorbed by GelMA may enhance the mechanical properties by achieving higher crosslinking, this is not always ideal. A high mechanical strength often compromises cell viability and proliferation,²⁷⁻²⁹ and the excessive UV exposure can be detrimental to the encapsulated cells in GelMA.^{28,30-32} Furthermore, each component of the bioink, such as the concentrations of GelMA, lithium phenyl(2,4,6-trimethylbenzoyl) phosphinate (LAP), and PEDOT:SPSS, affects the crosslinking rate, adding an additional layer of complexity. Generalizing a model for the gel fraction thus requires analysis of an enormous dataset, highlighting the difficulty of balancing multiple parameters to achieve the desired hydrogel properties.

Machine learning (ML) techniques offer significant potential in optimizing both the formulation of GelMA-PEDOT:SPSS hydrogels and the bioprinting process itself. ML algorithms can analyze vast datasets to identify patterns, predict outcomes, and optimize parameters more efficiently than traditional methods.³³⁻³⁹ ML is widely used in material science for characterization and optimization of synthesis processes.⁴⁰⁻⁴² By utilizing ML, researchers can explore the parameter space, optimize the formulation, and predict the performance of the hydrogels under various conditions.^{43,44} In addition, ML can be applied to optimize

3D bioprinting process, improving print accuracy, speed, and resolution, while reducing material waste.^{45,46} This approach can lead to the creation of highly customized and optimized biomaterials for specific tissue engineering applications, ultimately enhancing the effectiveness and precision of 3D bioprinting technologies. The large number of factors for the gel fraction makes it difficult to determine a model analytically or with traditional empirical methods. In such cases, ML is an attractive method to solve the problem.

Therefore, in this work, we used ML to optimize the curing of GelMA-PEDOT:SPSS hydrogels by predicting the gel fraction from three different feature groups. The purpose of the three feature groups is to understand the importance of different types of features on the prediction accuracy and for different real-world applications. Feature Group 1 utilizes bioink formulation and crosslinking parameter as input. This is useful to predict the gel fraction before the experiment as the optimized parameter for the desired gel fraction can be selected without a wide range of experiment, aiding in saving material cost and shortening experiment time. Feature Groups 2 and 3 predict the gel fraction without the prior crosslinking parameter. Feature Group 2 has absorption coefficient only as the input for ML model, while feature Group 3 is a combination of bioink formulation and absorption coefficient. The usage of absorption coefficient with no crosslinking parameter as input in feature Groups 2 and 3 will be significant for *in situ* monitoring for gel fraction. In real application, the UV power intensity and the UV exposure duration will most likely be different from the input setting due to imperfection of machine or human error. By predicting the gel fraction with the measurement of absorption coefficient instead of crosslinking parameter, the gel fraction can be fine-tuned in real time with a non-destructive method to improve the precision of the sample, at a relatively low cost as only a UV sensor is required for the measurement.

2. Methods

2.1. Synthesis of GelMA

GelMA was synthesized according to previously procedures described by Loessner *et al.*⁴⁷ Methacrylic anhydride (Sigma-Aldrich) of 1.4 mL was added dropwise into a 10% w/v gelatin type A (bloom strength 300, Sigma-Aldrich) solution dissolved in 100 mL of 1× phosphate-buffered saline (1× PBS, pH 7.2, Vivantis). The solution was stirred at 400 rpm while maintaining a temperature at 50°C, and 400 mL of 1× PBS was added to quench the reaction after 3 h. The mixture was transferred into 50 mL tubes and centrifuged at 3500× g for 3 min. The clear supernatant was transferred into 12 – 14 kDa cut-

off dialysis tubes and dialyzed against deionized water for 7 days at 40°C to remove unreacted methacrylic anhydride and by-products from the initial reaction. After dialysis, the GelMA solution was lyophilized for 7 days. Lyophilized GelMA was kept at –20°C in the refrigerator until further use. The chemical process for the synthesis of GelMA is illustrated in Figure 1A.

2.2. Preparation of varying opacity samples

PEDOT:SPSS (Clevios PH1000, Heraeus) was adjusted to the desired concentration stated in Table 1 using deionized water. Lyophilized GelMA was added to the PEDOT:SPSS solution and held at 37°C for 3h to ensure fully dissolved. Subsequently, LAP (L0290, TCI) was added to the GelMA-PEDOT:SPSS solution. The GelMA-PEDOT:SPSS solution was casted into a cylindrical mold to yield samples with 8 mm diameter, and 2 mm height. The sample will be crosslinked with UV light as shown in Figure 1B.

2.3. Data collection for gel fraction

2.3.1. Experiment setup

A high-intensity spot-curing system, Dymax BlueWave QX4, equipped with a 405 nm LED wand (VisiCure LED head, 405 nm), was used as the UV light source. UV light transmission through the hydrogel was measured using a UV light sensor (S120VC, Thorlabs) covered with a square pinhole with a size of 1 mm × 1 mm (S1000QK, Thorlabs), connected to an optical power and energy meter console (PM400, Thorlabs). The LED wand was mounted on a retort stand and positioned directly above the UV light sensor. The power output is controlled by adjusting the height of the LED wand. For the mold setup, a clean glass slide was used as the base beneath the mold. Two clips were used for the securing of the mold to prevent liquid leakage from between the mold and the glass slide, as seen in Figure 2A. Post-crosslinking, the clips were removed to separate the mold from the glass slide for hydrogel extraction, as shown in Figure 2B.

2.3.2. Crosslinking of GelMA-PEDOT:SPSS hydrogel

The prepared and mixed hydrogel solution (120 µL) was pipetted into the assembled mold setup. The mold was placed above the UV light sensor, as shown in Figure 2C, while curing the sample, to record the change in the received UV intensity during the crosslinking process. The UV light was shone on the mold for a specified power and duration, allowing for the photopolymerization process to occur. After the crosslinking process, the hydrogel was removed from the mold and transferred into a 35 mm petri dish of known mass, m_p . The experiment was repeated three times for every combination of bioink formulations, UV power intensity, and UV duration

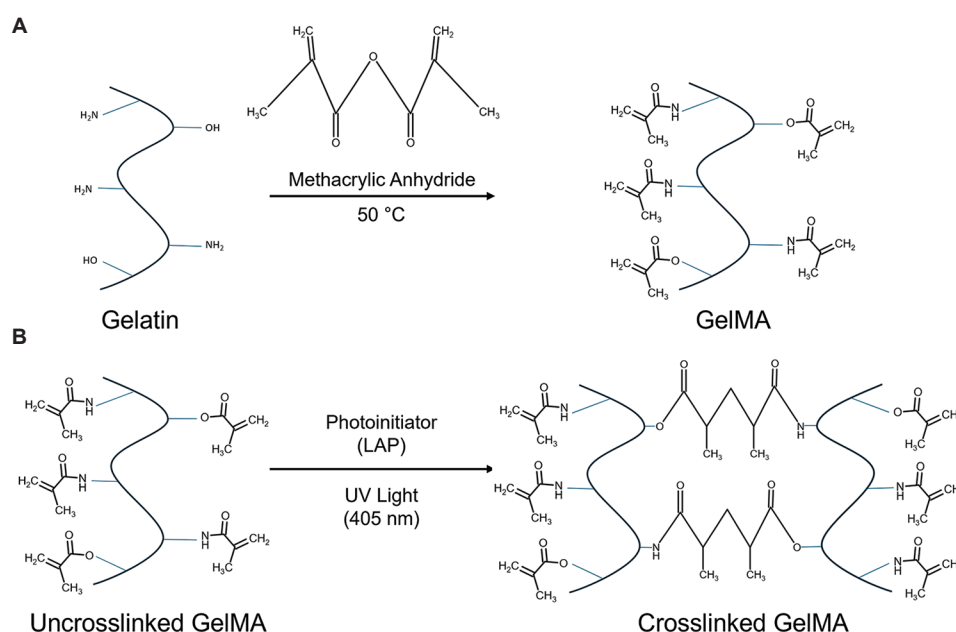


Figure 1. Chemical reaction for the synthesis and crosslinking of GelMA. (A) Schematic of the synthesis of GelMA. (B) Schematic of the crosslinking of GelMA.

Table 1. Bioink formulation and crosslinking parameters used in the experiment

GelMA (% w/v)	LAP (% w/v)	PEDOT: PSS (mg/mL)	UV Power intensity (mW/mm ²)	UV Duration (s)
10, 15	0.1, 0.3	0.5, 1.5, 3.0	0.5, 1.0	15, 30, 60

Abbreviations: LAP: Lithium phenyl (2,4,6-trimethylbenzoyl) phosphinate (LAP); GelMA: Gelatin methacryloyl; UV: Ultraviolet; PEDOT: PSS: Poly (3,4-ethylenedioxythiophene) polystyrene sulfonate.

stated in Table 1. All the petri dishes containing the hydrogel were lyophilized for 1 day. The mass of the lyophilized hydrogel with the petri dish was recorded as m_{h1} . $1\times$ PBS solution was then added into the petri dish, fully submerging the lyophilized hydrogel in PBS. The samples were placed into the 37°C oven for 5 h to allow the uncured hydrogel to dissolve. The PBS solutions with the dissolved uncured hydrogel were then removed with a pipette, the remaining cured hydrogel is shown in Figure 2D. The hydrogel was lyophilized for another 1 day. The lyophilized hydrogel is as shown in Figure 2E. The mass of the lyophilized hydrogel was measured and recorded as m_{h2} . The mass was utilized to calculate the gel fraction.

2.3.3. Gel fraction

Gel fraction is used to indicate the amount of crosslinking in the sample. It is defined as the mass of the crosslinked sample over the mass of the entire sample. As the uncured hydrogel is dissolved and removed, the gel fraction of the sample after the crosslinking process is calculated using the following formula (Equation I):

$$\text{Gel fraction (\%)} = \frac{\text{Mass of lyophilized undissolved hydrogel}}{\text{Mass of lyophilized hydrogel before dissolving}}$$

$$= \frac{m_{h2} - m_p}{m_{h1} - m_p} \quad (I)$$

2.3.4. Absorption coefficient

As the UV light passes through the sample, the photons are absorbed and scattered by the particles in the sample, as illustrated in Figure 2F. The strength of this effect can be quantified by the absorption coefficient. The absorption coefficient of the sample is calculated with the Beer-Lambert law (Equation II):

$$I = I_0 e^{-ax} \quad (II)$$

where I is the UV power intensity measured by the UV sensor through the sample, as shown in Figure 2G; I_0 is the UV power intensity measured when there is no sample on the UV sensor, as depicted in Figure 2H; x is the thickness

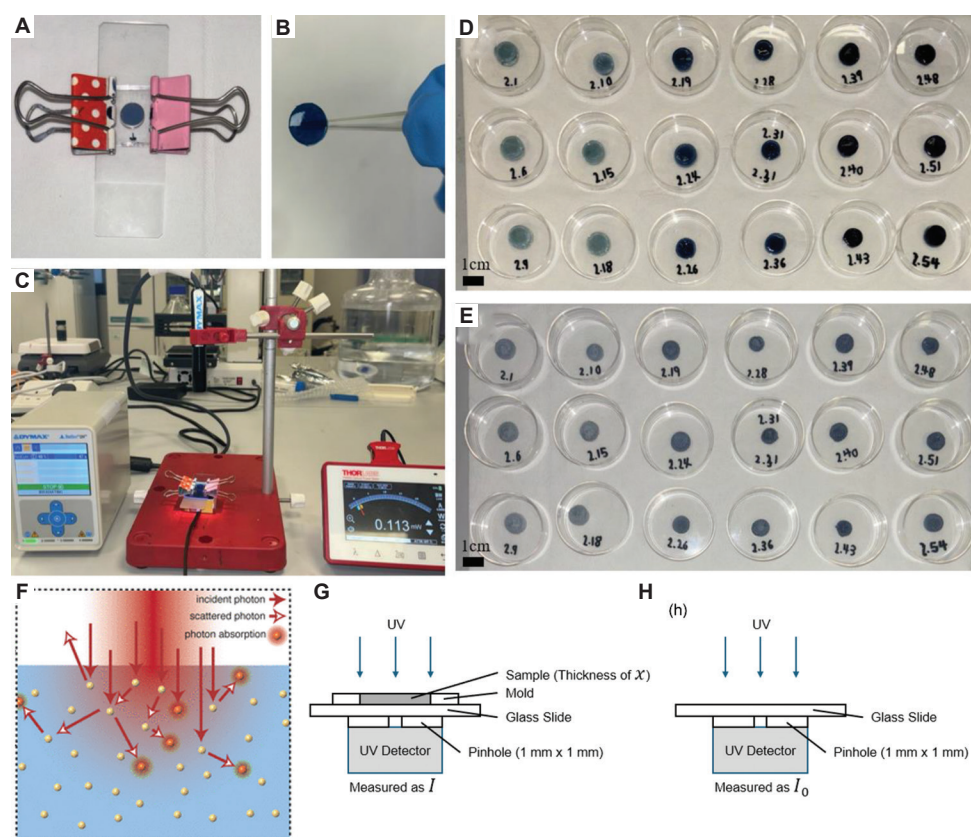


Figure 2. Experimental setup used in this work. (A) Mold filled with the bioink and secured by clip. (B) Crosslinked GelMA-PEDOT:SPSS hydrogel. (C) Experimental setup for the photopolymerization process of the hydrogel. (D) Hydrogels with different bioink formulation and crosslinking parameters after the uncured hydrogel is removed. (E) Lyophilized hydrogel. (F) Diagrams of photons scattered and absorbed by the particles in the sample. Adapted with permission from. Hogan *et al.*⁴⁹ Copyright© 2014 American Chemical Society. (G) Measurement of UV power intensity through the sample, I . (H) Measurement of the original UV power intensity without the sample, I_0 . Abbreviations: GelMA: Gelatin methacryloyl, UV: Ultraviolet, PEDOT:SPSS: Poly(3,4-ethylenedioxythiophene) polystyrene sulfonate.

of the sample (2 mm in this work); and a is the absorption coefficient. The equation can be rearranged to the following (Equation III) to calculate the absorption coefficient:

$$a = -\frac{1}{x} \ln \frac{I}{I_0} \quad (\text{III})$$

2.4. ML technique

In this study, ML techniques were utilized to understand the relationship between the gel fraction with the bioink formulation, crosslinking parameters, and absorption coefficients. Bioink formulation consists of three separate features in the dataset: GelMA concentrations, LAP concentrations, and PEDOT:SPSS concentrations. Crosslinking parameters are represented by two features, the UV power intensity, and the exposure duration during the photopolymerization process. The features are categorized into three groups as shown in Figure 3A. Feature Group 1 consists of bioink formulation and crosslinking parameters.

Features Group 2 has only one feature, *that is*, the absorption coefficient. Features Group 3 is the combination of bioink formulation and the absorption coefficient.

The algorithms used in this work were linear regression (LR), support vector regression (SVR), decision tree regressor (DTR), random forest regression (RFR), and deep neural network (DNN). Both LR and SVR are regression-based models, where LR assumes a linear model, while SVR is a non-linear model as radial basis function (RBF) kernel is being utilized. DTR and RFR are decision tree-based models, where DTR is the basic for the decision tree-based technique, while ensemble method is used by RFR to improve the accuracy of decision tree with the tradeoff of low readability. DNN was included in the test as it outperforms the traditional ML methods given sufficient sample count. Scikit-learn⁵⁰ was utilized to implement the ML models, while PyTorch was used for the implementation of the DNN model. The suitability of regression-based

techniques, decision tree-based techniques, and neural networks in predicting the gel fraction was compared. The brief introduction and the tuning parameters for the models are detailed in the following section.

2.4.1. LR

The LR technique was selected for its simplicity and interpretability. LR is ideal for identifying and quantifying linear relationships between inputs and outputs. Its straightforward nature provides a baseline model for comparison with more complex algorithms. In addition, when the relationship between variables is approximately linear, LR can deliver fast and reliable predictions. The LR model, represented in Equation IV, is fitted using the ordinary least square method. In this work, x_{GelMA} , x_{LAP} , and x_{PEDOT} are the concentration of GelMA, LAP, and PEDOT:SPSS, respectively. x_p is the UV power intensity, x_t is the UV duration, and x_a is the absorption coefficient. ω are the coefficients to be fitted.

$$y_{Gel} = \omega_{GelMA} x_{GelMA} + \omega_{LAP} x_{LAP} - \omega_{PEDOT} x_{PEDOT} + \omega_p x_p + \omega_t x_t + \omega_a x_a \quad (IV)$$

$\omega_p x_p + \omega_t x_t$ was replaced with $\omega_a x_a$ in feature groups 2 and 3, while $\omega_{GelMA} x_{GelMA} + \omega_{LAP} x_{LAP} - \omega_{PEDOT} x_{PEDOT}$ was removed in feature group 2.

2.4.2. SVR

The SVR model, a widely used ML regression technique, was employed to compare its accuracy with the LR model as both are regression-based methods. SVR enhances performance over LR in the presence of outliers by maximizing the number of data points within the hyperplane area.⁵¹ To achieve a non-LR, the RBF kernel was utilized. The regularization parameter C was set to 993 and γ to 0.57 for feature Group 1, while C was 130 and γ was 0.53 for feature Groups 2 and 3. The gamma was set to “scale” for all feature groups ($1/(n_features * X.var())$), and the tolerance for the stopping criterion was 0.001.

2.4.3. Decision tree regression

DTR was selected for its adeptness at mapping complex decision paths based on input parameters. Unlike regression-based techniques, decision trees excel at

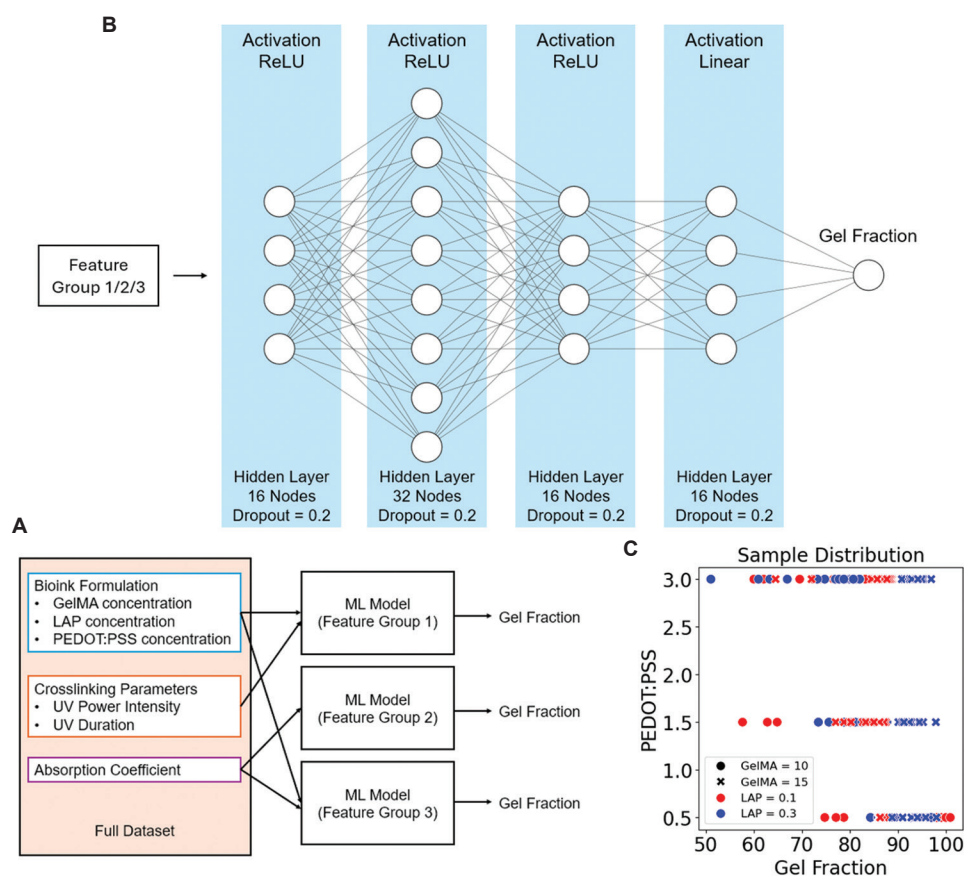


Figure 3. Details of machine learning (ML) models. (A) The three different feature groups used to train the ML models. (B) Architecture of the deep neural network model. (C) Sample distribution

capturing non-monotonic relationships between variables, which are prevalent in systems when the variables interact non-additively. The hierarchical structure of decision trees is particularly useful for decomposing the decision process into a series of simple rules, offering invaluable insights into the relationships between parameters. The mean squared error (MSE) criterion was used for splitting, employing the “best split” approach to optimize the decision tree.

2.4.4. RFR

RFR constructs multiple DTR using subsets of the dataset and averages their outputs to predict the target variable.⁵² This approach improves accuracy and reduces overfitting compared to a single DTR. However, RFR models are challenging to visualize and interpret. The criterion for splitting used is MSE. The number of trees in the forest was set as 15.

2.4.5. DNN

DNN outperforms traditional regression and decision tree methods in conventional ML technique by automatically extracting complex features, handling non-linear relationships, and scaling effectively with large and high-dimensional datasets. While regression models such as LR or SVR are limited by their linear assumptions and decision trees-based models such as DTR or RFR often risk overfitting, DNN leverages multiple layers of non-linear transformations to capture intricate patterns in data. However, DNN will perform worse than conventional ML techniques when the sample count is low.

The architecture of the DNN model used in this work is illustrated in [Figure 3B](#). It has four hidden layers, with 16 nodes in the first hidden layer, 32 nodes in the second hidden layer, and 16 nodes in both the third and fourth hidden layers. ReLU activation was used for the first, second, and third hidden layers. The fourth hidden layer utilized a linear activation instead. To prevent overfitting, dropout with a rate of 0.2 was applied between each hidden layer. The model was trained using standard backpropagation and optimized with the Adam optimizer. The loss function used was mean absolute percentage error (MAPE).

2.5. ML training procedure

The distribution of the gel fraction for 287 samples obtained from the experiment in this work is depicted in [Figure 3C](#). There are six features and one label in the dataset. The six features are GelMA concentration, LAP concentration, PEDOT:SPSS concentration, UV power intensity, UV duration, and absorption coefficient, with the gel fraction as the label or output for the ML model. Every feature in the dataset was normalized with a MinMaxScaler, which transformed every feature to a range of 0 – 1. The sample was then randomly split in a 70:20:10 ratio into training

set (200 samples), validation set (58 samples), and testing set (29 samples). The training set was used for training for the ML model, and the performance was tested against the validation set.⁵³ The testing set was kept untouched until the end of all training to verify the effectiveness of the models. Both MAPE and coefficient of determination (R^2) were used as the performance criteria for model validation. MAPE was selected over other criteria such as MSE or mean absolute error as the percentage error gives a better interpretability on how much the prediction deviates from the real value. Meanwhile, R^2 is dimensionless and can be used to compare the performance of different models, as an R^2 closer to 1 for a model indicates a better fit. All the hyperparameters stated in sections 2.4.1 to 2.4.5 were tuned with grid search method, while the default value was used for the unmentioned parameters.

Each of the ML techniques described in section 2.4 was trained against the gel fraction with feature Groups 1, 2, and 3 as the input. The best ML technique for each feature group was verified with the testing set.

3. Results and discussion

[Figure 4A](#) demonstrates that all variables in the dataset influence the resulting gel fraction. Higher concentrations of GelMA and LAP facilitate faster curing of the ink ($P < 0.05$ for both in one tailed t -test), thereby increasing the gel fraction. In addition, greater UV power and longer exposure duration enhance the UV energy received by the photoinitiator ($P < 0.05$ for UV power, $P < 0.15$ for UV duration), leading to more crosslinking. Conversely, the higher concentration of PEDOT:SPSS in the ink obstructs the UV light from activating the photoinitiator, resulting in reduced crosslinking and a lower gel fraction ($P < 0.25$).

The Spearman correlation shown in [Figure 4B](#) corroborates these observations. According to the correlation data, PEDOT:SPSS concentration has the most significant impact on the gel fraction, followed by the concentrations of GelMA, UV duration, UV power, and LAP. The correlation coefficients are not particularly high, with the rank for PEDOT:SPSS concentration being -0.47 . This moderate level of correlation justifies the application of ML to better predict the gel fraction.

It is also noteworthy that the absorption coefficient of the samples is moderately related to the gel fraction, with a correlation coefficient of -0.42 . As observed in [Figure 4C](#), the UV intensity measured increases over time while the absorption coefficient decreases as the sample cures. This observation suggests the potential for using the absorption coefficient to perform *in situ* predictions of the gel fraction, a concept which will be further elaborated in section 3.2.

3.1. Prediction of gel fraction from bioink formulations and crosslinking parameters

The performance metrics for each ML technique used to train the model are presented in Table 2. SVR exhibited the best performance, achieving an MAPE of 3.13%, a standard deviation (SD) of 3.75%, and a coefficient of determination (R^2) of 0.79. These results indicate that the model has a very good fit and can accurately predict the gel fraction. In contrast, LR demonstrated the lowest accuracy, with an MAPE of 6.28%, an SD of 4.61%, and the lowest R^2 at 0.41. Nonetheless, this still represents a reasonably good accuracy, suggesting that the input features provide sufficient information to predict the gel fraction effectively.

Although LR provides the lowest accuracy, it is valuable for gaining insights into the relationships between variables. The LR model can be summarized by Equation V:

$$Gel(\%) = 1.719x_{GelMA} + 17.26x_{LAP} - 3.814x_{PEDOT} + 9.560x_p + 0.1064x_t + 56.29 \quad (V)$$

From the equation, it can be inferred that the increase in GelMA concentration, LAP concentration, UV power, and UV duration will result in a higher gel fraction. Conversely, an increase in the concentration of PEDOT:SPSS will lower the resultant gel fraction. These findings are consistent with the conclusions drawn from the Spearman correlation analysis.

Figure 5 illustrates the plot of predicted gel fraction against actual gel fraction for the validation dataset. Although the LR models exhibited lower overall accuracy, it accurately predicted an outlier circled in red, a feat not achieved by the other four models. Conversely, LR struggled to predict the gel fraction at the lower end of the dataset, as indicated by the blue circle, where the other models performed accurately. This discrepancy was likely

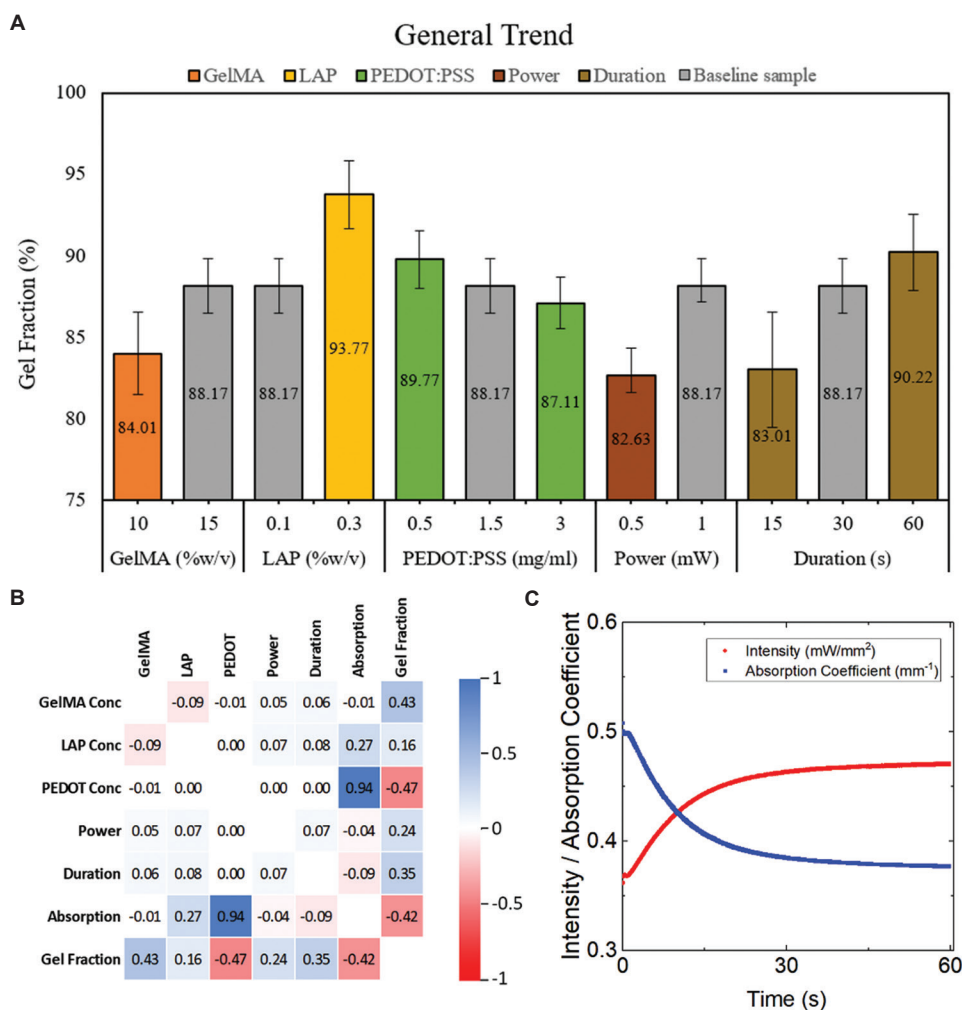


Figure 4. Relationship between the variables in the dataset. (A) Trend of average gel fraction by varying the individual curing parameters. (B) Spearman correlation of all the variables in the dataset. (C) Ultraviolet intensity measured and the absorption coefficient of a sample over time during the curing operation

Table 2. Performance of different machine learning models in predicting gel fraction from GelMA concentration, LAP concentration, PEDOT: PSS concentration, UV power, and UV duration

	MAPE (%)	SD (%)	R ²
Linear regression	6.28	4.61	0.41
Decision tree regression	4.05	4.63	0.67
Random forest regression	3.42	3.99	0.76
Support vector regression	3.13	3.75	0.79
Deep neural network	3.81	3.70	0.74

Abbreviations: MAPE: Mean absolute percentage error; R²: Coefficient of determination; SD: Standard deviation, LAP: Lithium phenyl (2,4,6-trimethylbenzoyl) phosphinate (LAP), GelMA: Gelatin methacryloyl, UV: Ultraviolet, PEDOT: PSS: Poly (3,4-ethylenedioxythiophene) polystyrene sulfonate.

due to the similarity in features between the data points circled in red and blue. The predicted values within the red circle were very close to the 61% value in the blue circle for the other four models. The value in the red circle might be an outlier caused by incorrect measurement, with LR coincidentally providing accurate predictions by overestimating.

The DNN model achieved an MAPE of 3.81% and an R² of 0.74, which were close but slightly inferior to the performance of SVR and RFR models. However, the DNN model offers the potential for transfer learning, enabling its application to other types of samples with reduced training data requirements. The trained model can serve as the initial weight for training on other GelMA mixtures, or even hydrogel mixtures, enhancing its adaptability and efficiency.

The high accuracy of these models enables users to pre-select parameters tailored to achieve specific gel fractions, significantly streamlining the optimization process for 3D bioprinting. This capability reduces the need for extensive experimentation, thereby saving time and resources while enhancing precision in achieving the desired hydrogel properties.

3.2. Prediction of gel fraction through replacing the crosslinking parameters with absorption coefficient

From the Spearman correlation analysis, it was found that the gel fraction correlates with the absorption coefficient of the samples. This correlation implies that UV measurements of the GelMA samples could be utilized to determine the current gel fraction non-destructively. Furthermore, *in situ* measurements of the gel fraction could be performed during the curing process, thereby allowing more precise control over the gel fraction.

Two different types of feature groups were trained with different ML techniques to compare the effectiveness of the absorption coefficient in the prediction of gel fraction, with or without the information of sample composition (GelMA concentration, LAP concentration, PEDOT:SPSS concentration) as input. The performances of the models are shown in Table 3. While the MAPE of the models with just absorption coefficient was low at between 5.55% and 7.88% for different ML technique, the R² was very low with RFR being the best at 0.27. The R² of regression-based ML techniques such as LR and SVR was close to zero, at 0.03 and 0.02, respectively. In contrast, the decision tree-based ML techniques had higher R², with DTR at 0.25 and RFR at 0.27. This indicates that the absorption coefficient alone does not have a linear relationship with the gel fraction, and the general low R² implies that the noise is too large.

When the information of sample composition was included, the performance of the models improved significantly. DTR had the lowest MAPE at 3.13%, with an R² of 0.67. RFR had the best R² of 0.72 while having an MAPE of 3.79%. The huge improvement in the accuracy showed that the input of sample's composition is vital for a better prediction. Similar to the model without the sample information, the decision tree-based techniques had a better performance when compared to the regression-based techniques. The increase in R² for the regression-based techniques could be attributed to the sample composition having a more linear relationship with the gel fraction. However, the lower R² for the regression-based techniques when compared to the feature Group 1 further proved that a monotonic relationship does not exist between the absorption and the gel fraction, as swapping the absorption coefficient to UV power and UV exposure duration can improve the R² to 0.79 for SVR.

From Figure 6A, LR, SVR, and DNN failed to generalize the gel fraction when it was lower than 80%. Meanwhile, DTR and RFR could predict the gel fraction at higher accuracy at that region. When the bioink formulation was included as in Figure 6B, the performance was generally improved, but LR, SVR, and DNN were still having difficulty to predict the gel fraction at below 70%. The DNN model shared a similar outcome with the LR or SVR as there was not much data points at lower gel fraction, thus the DNN was unable to generalize the lower value.

The good accuracy of the ML model trained from feature Group 3 makes it suitable for situations where the bioink formulation of the GelMA is known, but the crosslinking intensity and the exposure duration of a specific area are unknown, such as when the UV spot size is relatively small compared to the entire GelMA construct, or when the

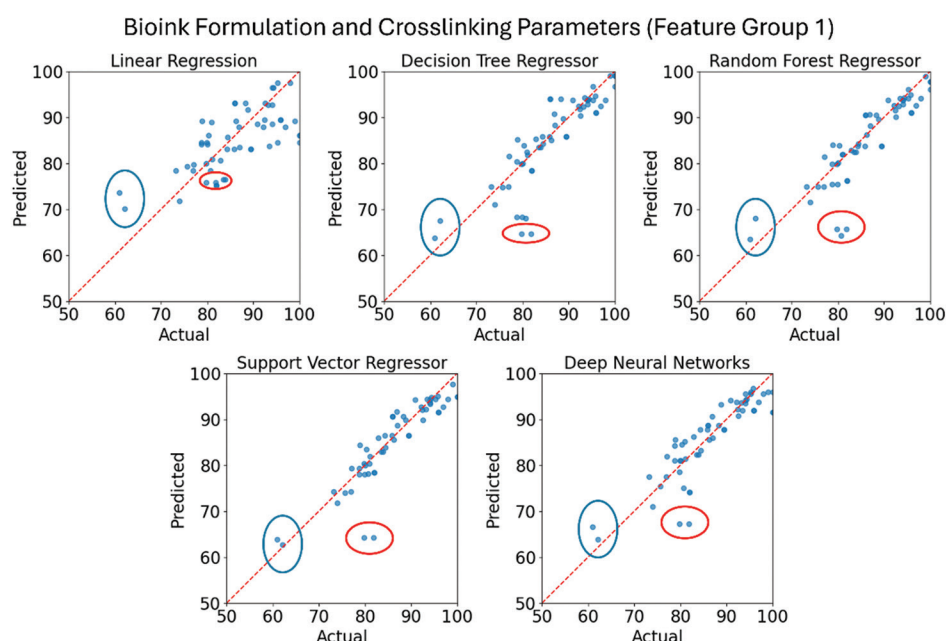


Figure 5. Graphs of predicted values of gel fraction against actual values, for different machine learning models used to predict gel fraction from GelMA concentration, LAP concentration, PEDOT:SPSS concentration, UV power, and UV duration. Red circle and blue circle represent the outliers consisting of the same data points.

Abbreviations: LAP: Lithium phenyl(2,4,6-trimethylbenzoyl) phosphinate (LAP); GelMA: Gelatin methacryloyl; UV: Ultraviolet; PEDOT:SPSS: Poly(3,4-ethylenedioxythiophene) polystyrene sulfonate.

Table 3. Performance of different machine learning models for predicting gel fraction based on absorption coefficient

Algorithm	Without sample info			With sample info		
	MAPE (%)	SD (%)	R ²	MAPE (%)	SD (%)	R ²
Linear regression	7.88	9.11	0.03	6.58	7.16	0.38
Decision tree regression	5.55	7.21	0.25	3.13	5.94	0.67
Random forest regression	6.35	6.68	0.27	3.79	5.33	0.72
Support vector regression	7.31	9.35	0.02	4.97	7.41	0.53
Deep neural network	7.43	8.88	0.09	5.93	6.33	0.50

Abbreviations: MAPE: Mean absolute percentage error; R²: Coefficient of determination; SD: Standard deviation.

crosslinking process is stopped abruptly. By measuring the absorption coefficient, the gel fraction of that specific area can be predicted.

3.3. Model validation

The model with the best R² from each feature group was validated using an untouched testing dataset. The performance for the best ML model in each feature group is shown in Table 4. For feature Group 1, the performance of SVR remained consistently high at an R² of 0.79. However, for feature Group 2, where only the absorption coefficient was used as the input for the model, the performance of the models was low compared to the validation dataset, with an R² of 0.02. This suggests

that the model trained was being overfitted, as absorption coefficient alone was not enough to predict the gel fraction accurately. In feature Group 3, while RFR was the model with the best performance, its R² was lowered from 0.72 to 0.41 in the testing dataset. This suggests that there was some overfitting in the RFR model in feature Group 3 too. It is noteworthy that R² of the DNN model was relatively stable at 0.54 as compared to 0.50 of the validation datasets. Figure 7 shows that the models derived from feature Groups 2 and 3 will overestimate the gel fraction at below 70%, with DNN having a slightly better performance than RFR in that range. Meanwhile, the SVR model from feature Group 1 can predict the gel fraction accurately even at a lower range. This indicates

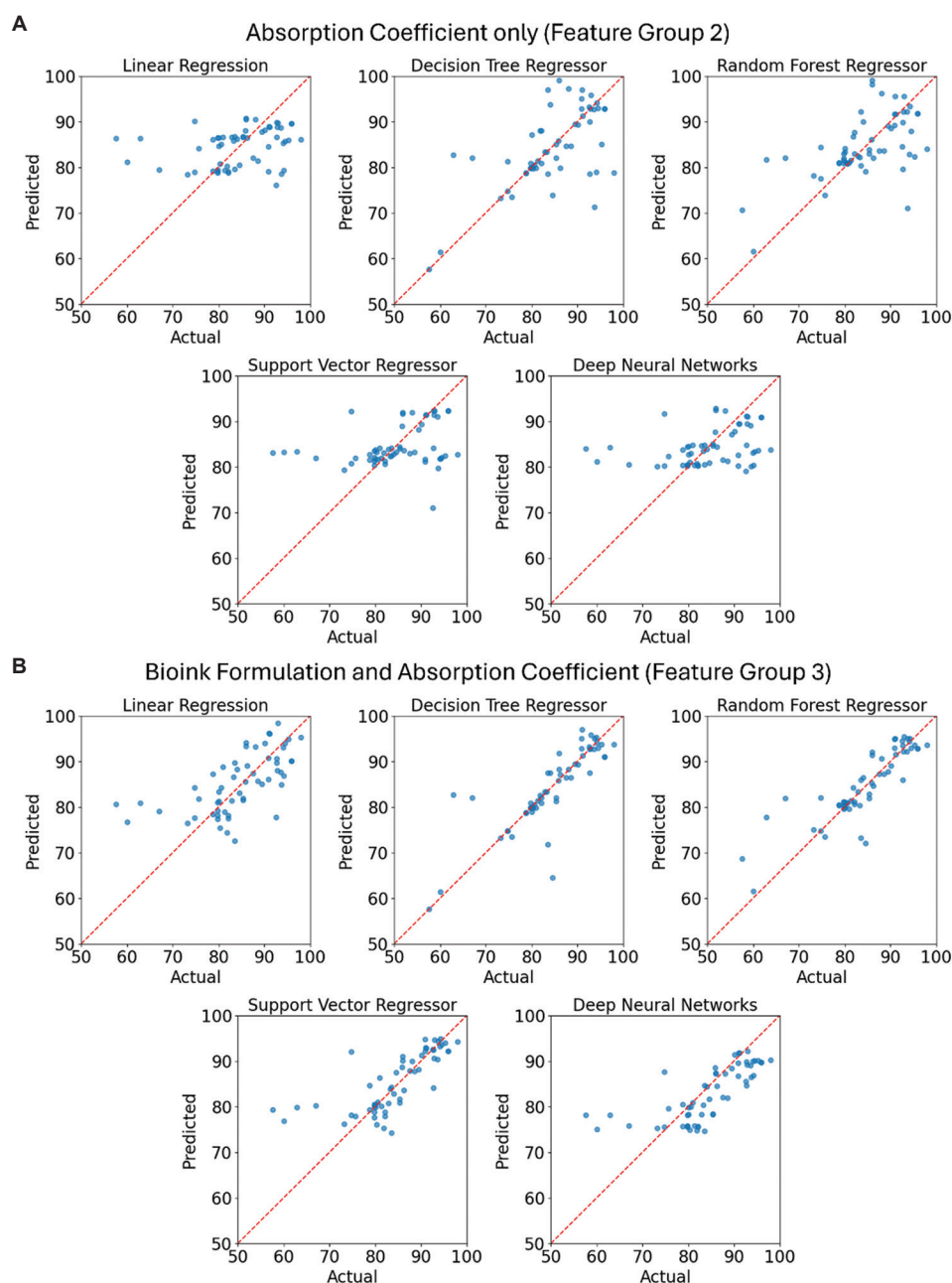


Figure 6. Graphs of predicted values of gel fraction against actual values, for different machine learning models used to predict the gel fraction based on absorption coefficient only (A), and absorption coefficient and bioink formulation of the ink (B)

that feature Group 1 provides enough information to estimate the gel fraction at the lower range, even with a relatively low sample size.

3.4. Limitations

This study acknowledges the lack of data points from the lower gel fraction, with less than 10% of the data points below 70% gel fraction, rendering the estimation of gel fraction at below 70% by the models from feature

Groups 2 and 3 inaccurate. Extrapolation beyond the boundaries of the input variables may not yield reliable results. Furthermore, this model is limited to sample with a thickness of 2 mm. In future research, it is necessary to widen the range of the data, such that the dataset consists of samples with gel fraction from 0% to 100% and with different hydrogel thickness, so as to improve the reliability and the accuracy of the model.

Table 4. Performance of the best machine learning models from each feature group in predicting gel fraction

	MAPE (%)	SD (%)	R ²
Feature Group 1			
Support vector regression	3.13	3.75	0.79
Feature Group 2			
Random forest regression	9.10	9.92	0.02
Feature Group 3			
Random forest regression	6.75	8.56	0.41
Deep neural network	6.31	5.78	0.54

Abbreviations: MAPE: Mean absolute percentage error; R²: Coefficient of determination; SD: Standard deviation.

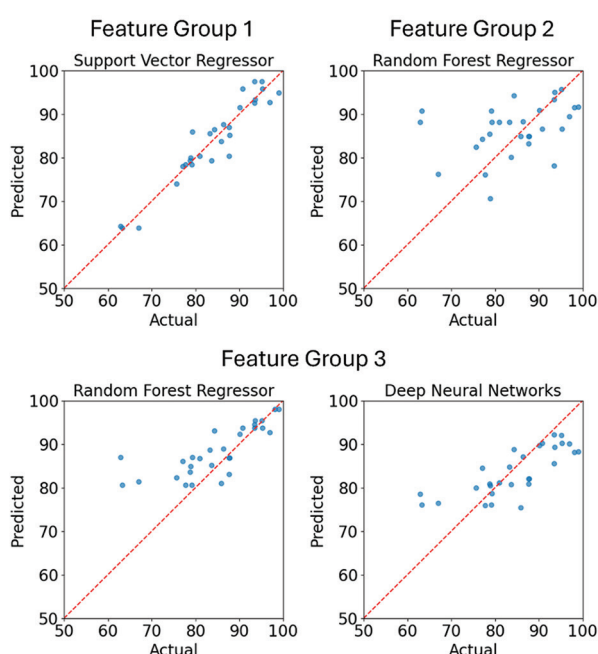


Figure 7. Graphs of predicted values of gel fraction against actual values for the testing dataset

Besides, this model assumed that no additional layer is added on the sample after the crosslinking process. This model is not suitable in a situation where the transmittivity of the hydrogel is too low, which necessitates curing after every layer. This could be solved by utilizing a recurrent neural network by having the curing information from the previous layer as the input for the prediction in the new layer.

Furthermore, this model is limited to GelMA-PEDOT:SPSS hydrogel. While this concept can be used to train an ML model for a different hydrogel, it is preferable to have a model that can be generalized for all hydrogels. A possible solution is to use transfer learning to reduce the

sample size needed for the other hydrogel model. Common properties for the crosslinking of polymer such as monomer reactivity ratio and extent of reaction can be included in the dataset for a more robust DNN model where the learnt knowledge can be transferred easily between models.

4. Conclusion

This study demonstrates the feasibility of predicting the gel fraction of GelMA-PEDOT:SPSS hydrogels using ML models based on bioink formulation and crosslinking parameters. SVR emerges as the best-performing model, with an MAPE of only 3.13%. This high accuracy minimizes the time and material costs typically associated with optimizing hydrogel properties to achieve the required gel fraction. Furthermore, by replacing crosslinking parameters with absorption coefficient, we demonstrated the potential for estimating gel fraction without prior crosslinking information. The DNN model achieved an MAPE of 6.31% for this scenario, indicating its utility for *in situ* gel fraction measurements via a UV detector. This capability can significantly enhance the fine-tuning of GelMA-PEDOT:SPSS hydrogel properties during 3D bioprinting by allowing non-destructive, real-time measurement of the gel fraction. Overall, this work contributes to reducing experimental costs and improving the precision of hydrogel crosslinking, enabling a more efficient process in hydrogel-related research. Consequently, this accelerates advancements in the field of tissue regeneration, providing a robust foundation for future studies and applications.

Future work should explore the relationship between gel fraction and various hydrogel properties, such as rheological behavior, mechanical strength, and cell viability. Integrating these data with the current models will enable users to select optimal parameters tailored to specific applications. Furthermore, the ML models should be validated in a 3D printer to demonstrate its effectiveness in optimizing the crosslinking of hydrogel during 3D printing. This research lays the groundwork for more efficient and effective design of hydrogels, enabling advancements in 3D bioprinting and other critical applications in biotechnology.

Acknowledgments

None.

Funding

This research is supported by the National Research Foundation for NRF Investigatorship Award No.: NRF-NRFI07-2021-0007.

Conflict of interest

Wai Yee Yeong is an Editorial Board Member of this journal, but was not in any way involved in the editorial and peer-review process conducted for this paper, directly or indirectly. Separately, other authors declared that they have no known competing financial interests or personal relationships that could have influenced the work reported in this paper.

Author contributions

Conceptualization: Xi Huang, Guo Liang Goh

Investigation: Xi Huang, Ye Xuan Wong

Methodology: Xi Huang, Ye Xuan Wong, Guo Liang Goh, Xinchao Gao, Jia Min Lee

Writing – original draft: Xi Huang, Ye Xuan Wong, Guo Liang Goh, Xinchao Gao, Jia Min Lee

Writing – review & editing: All authors

Ethics approval and consent to participate

Not applicable.

Consent for publication

Not applicable.

Availability of data

Data are available from the corresponding authors on reasonable request.

References

- Wales DJ, Keshavarz M, Howe C, Yeatman E. 3D printability assessment of poly(octamethylene maleate (anhydride) citrate) and poly(ethylene glycol) diacrylate copolymers for biomedical applications. *ACS Appl Polym Mater.* 2022;4(8):5457–5470.
doi: 10.1021/acsapm.2c00531
- Dutta SD, Ganguly K, Hexiu J, Randhawa A, Moniruzzaman M, Lim KT. A 3D bioprinted nanoengineered hydrogel with photoactivated drug delivery for tumor apoptosis and simultaneous bone regeneration via macrophage immunomodulation. *Macromol Biosci.* 2023;23(9):2300096.
doi: 10.1002/mabi.202300096
- Ganguly S, Margel S. 3D printed magnetic polymer composite hydrogels for hyperthermia and magnetic field driven structural manipulation. *Prog Polym Sci.* 2022;131:101574.
doi: 10.1016/j.progpolymsci.2022.101574
- Kurian AG, Singh RK, Patel KD, Lee JH, Kim HW. Multifunctional GelMA platforms with nanomaterials for advanced tissue therapeutics. *Bioact Mater.* 2022;8:267–295.
doi: 10.1016/j.bioactmat.2021.06.027
- Yang X, Sun X, Liu J, *et al.* Photo-crosslinked GelMA/collagen membrane loaded with lysozyme as an antibacterial corneal implant. *Int J Biol Macromol.* 2021;191:1006–1016.
doi: 10.1016/j.ijbiomac.2021.09.144
- Shin SR, Zihlmann C, Akbari M, *et al.* Reduced graphene oxide-gelMA hybrid hydrogels as scaffolds for cardiac tissue engineering. *Small.* 2016;12(27):3677–3689.
doi: 10.1002/sml.201600178
- Ku SH, Lee SH, Park CB. Synergic effects of nanofiber alignment and electroactivity on myoblast differentiation. *Biomaterials.* 2012;33(26):6098–6104.
doi: 10.1016/j.biomaterials.2012.05.018
- Rowlands AS, Cooper-White JJ. Directing phenotype of vascular smooth muscle cells using electrically stimulated conducting polymer. *Biomaterials.* 2008;29(34):4510–4520.
doi: 10.1016/j.biomaterials.2008.07.052
- Zhu W, Ye T, Lee SJ, *et al.* Enhanced neural stem cell functions in conductive annealed carbon nanofibrous scaffolds with electrical stimulation. *Nanomedicine.* 2018;14(7):2485–2494.
doi: 10.1016/j.nano.2017.03.018
- Chen C, Bai X, Ding Y, Lee IS. Electrical stimulation as a novel tool for regulating cell behavior in tissue engineering. *Biomater Res.* 2019;23(1):25.
doi: 10.1186/s40824-019-0176-8
- Levin M, Stevenson CG. Regulation of cell behavior and tissue patterning by bioelectrical signals: Challenges and opportunities for biomedical engineering. *Annu Rev Biomed Eng.* 2012;14:295–323.
doi: 10.1146/annurev-bioeng-071811-150114
- Dvir T, Timko BP, Brigham MD, *et al.* Nanowired three-dimensional cardiac patches. *Nat Nanotechnol.* 2011;6(11):720–725.
doi: 10.1038/nnano.2011.160
- Irimia-Vladu M. “Green” electronics: Biodegradable and biocompatible materials and devices for sustainable future. *Chem Soc Rev.* 2014;43(2):588–610.
doi: 10.1039/C3CS60235D
- Sun K, Zhang S, Li P, *et al.* Review on application of PEDOTs and PEDOT: PSS in energy conversion and storage devices. *J Mater Sci Mater Electron.* 2015;26:4438–4462.
doi: 10.1007/s10854-015-2895-5
- Heo DN, Acquah N, Kim J, Lee SJ, Castro NJ, Zhang LG. Directly induced neural differentiation of human adipose-derived stem cells using three-dimensional culture system of conductive microwell with electrical stimulation. *Tissue Eng Part A.* 2018;24(7–8):537–545.

- doi: 10.1089/ten.TEA.2017.0150
16. Spencer AR, Shirzaei Sani E, Soucy JR, *et al.* Bioprinting of a cell-laden conductive hydrogel composite. *ACS Appl Mater Interfaces*. 2019;11(34):30518-30533.
doi: 10.1021/acsami.9b07353
 17. Lee JJ, Ng HY, Lin YH, *et al.* The 3D printed conductive grooved topography hydrogel combined with electrical stimulation for synergistically enhancing wound healing of dermal fibroblast cells. *Biomater Adv*. 2022;142:213132.
doi: 10.1016/j.bioadv.2022.213132
 18. Spencer AR, Primbetova A, Koppes AN, Koppes RA, Fenniri H, Annabi N. Electroconductive gelatin methacryloyl-PEDOT: PSS composite hydrogels: Design, synthesis, and properties. *ACS Biomater Sci Eng*. 2018;4(5):1558-1567.
doi: 10.1021/acsbmaterials.8b00135
 19. Zhang S, Chen Y, Liu H, *et al.* Room-temperature-formed PEDOT: PSS hydrogels enable injectable, soft, and healable organic bioelectronics. *Adv Mater*. 2020;32(1):1904752.
doi: 10.1002/adma.201904752
 20. Fu F, Wang J, Zeng H, Yu J. Functional conductive hydrogels for bioelectronics. *ACS Mater Lett*. 2020;2(10):1287-1301.
doi: 10.1021/acsmaterialslett.0c00309
 21. Sagdic K, Fernández-Lavado E, Mariello M, Akouissi O, Lacour SP. Hydrogels and conductive hydrogels for implantable bioelectronics. *MRS Bull*. 2023;48(5):495-505.
doi: 10.1557/s43577-023-00536-1
 22. Zhang H, Guo J, Wang Y, Sun L, Zhao Y. Stretchable and conductive composite structural color hydrogel films as bionic electronic skins. *Adv Sci (Weinh)*. 2021;8(20):2102156.
doi: 10.1002/advs.202102156
 23. Linde E, Celina MC, Appelhans LN, Roach DJ, Cook AW. *In situ* characterization of material extrusion printing by near-infrared spectroscopy. *Addit Manuf*. 2023;63:103420.
doi: 10.1016/j.addma.2023.103420
 24. Camposeo A, Arkadii A, Romano L, *et al.* Impact of size effects on photopolymerization and its optical monitoring *in-situ*. *Addit Manuf*. 2022;58:103020.
doi: 10.1016/j.addma.2022.103020
 25. Vallabh CK, Zhang Y, Zhao X. *In-situ* ultrasonic monitoring for vat photopolymerization. *Add Manuf*. 2022;55:102801.
doi: 10.1016/j.addma.2022.102801
 26. El-Sherbiny IM, Yacoub MH. Hydrogel scaffolds for tissue engineering: Progress and challenges. *Glob Cardiol Sci Pract*. 2013;2013(3):316-342.
doi: 10.5339/gcsp.2013.38
 27. Wu Y, Xiang Y, Fang J, *et al.* The influence of the stiffness of GelMA substrate on the outgrowth of PC12 cells. *Biosci Rep*. 2019;39(1):BSR20181748.
doi: 10.1042/bsr20181748
 28. Pepelanova I, Kruppa K, Scheper T, Lavrentieva A. Gelatin-methacryloyl (GelMA) hydrogels with defined degree of functionalization as a versatile toolkit for 3d cell culture and extrusion bioprinting. *Bioengineering (Basel)*. 2018;5(3):55.
doi: 10.3390/bioengineering5030055
 29. Lantoine J, Grevesse T, Villers A, *et al.* Matrix stiffness modulates formation and activity of neuronal networks of controlled architectures. *Biomaterials*. 2016;89:14-24.
doi: 10.1016/j.biomaterials.2016.02.041
 30. Monteiro N, Thrivikraman G, Athirasala A, *et al.* Photopolymerization of cell-laden gelatin methacryloyl hydrogels using a dental curing light for regenerative dentistry. *Dent Mater*. 2018;34(3):389-399.
doi: 10.1016/j.dental.2017.11.020
 31. Annabi N, Tamayol A, Uquillas JA, *et al.* 25th anniversary article: Rational design and applications of hydrogels in regenerative medicine. *Adv Mater*. 2014;26(1):85-123.
doi: 10.1002/adma.201303233
 32. Fairbanks BD, Schwartz MP, Bowman CN, Anseth KS. Photoinitiated polymerization of PEG-diacrylate with lithium phenyl-2,4,6-trimethylbenzoylphosphine: Polymerization rate and cytocompatibility. *Biomaterials*. 2009;30(35):6702-6707.
doi: 10.1016/j.biomaterials.2009.08.055
 33. Goh GL, Huang X, Toh W, *et al.* Joint angle prediction for a cable-driven gripper with variable joint stiffness through numerical modeling and machine learning. *Int J AI Mater Des*. 2024;1(1):2328.
doi: 10.36922/ijamd.2328
 34. Goh GL, Goh GD, Pan JW, Teng PS, Kong PW. Automated service height fault detection using computer vision and machine learning for badminton matches. *Sensors*. 2023;23(24):9759.
doi: 10.3390/s23249759
 35. Goh GD, Lee JM, Goh GL, Huang X, Lee S, Yeong WY. Machine learning for bioelectronics on wearable and implantable devices: Challenges and potential. *Tissue Eng Part A*. 2023;29(1-2):20-46.
doi: 10.1089/ten.TEA.2022.0119
 36. Goh GL, Zhang H, Goh GD, Yeong WY, Chong TH. Multi-objective optimization of intense pulsed light sintering process for aerosol jet printed thin film. *Mater Sci Addit Manuf*. 2022;1(2):10.
doi: 10.36922/msam.26
 37. Sinha AK, Goh GL, Yeong WY, Cai Y. Ultra-low-cost,

- crosstalk-free, fast-responding, wide-sensing-range tactile fingertip sensor for smart gloves. *Adv Mater Interfaces*. 2022;9(21):2200621.
doi: 10.1002/admi.202200621
38. Liang F, Valdes JP, Cheng S, *et al*. Liquid-liquid dispersion performance prediction and uncertainty quantification using recurrent neural networks. *Ind Eng Chem Res*. 2024;63(17):7853-7875.
doi: 10.1021/acs.iecr.4c00014
39. Cheng S, Quilodrán-Casas C, Ouala S, *et al*. Machine learning with data assimilation and uncertainty quantification for dynamical systems: A review. *IEEE/CAA J Autom Sin*. 2023;10(6):1361-1387.
doi: 10.1109/JAS.2023.123537
40. Nathanael K, Cheng S, Kovalchuk NM, Arcucci R, Simmons MJ. Optimization of microfluidic synthesis of silver nanoparticles: A generic approach using machine learning. *Chem Eng Res Des*. 2023;193:65-74.
doi: 10.1016/j.cherd.2023.03.007
41. Xia Z, Ma K, Cheng S, *et al*. Accurate identification and measurement of the precipitate area by two-stage deep neural networks in novel chromium-based alloys. *Phys Chem Chem Phys*. 2023;25(23):15970-15987.
doi: 10.1039/D3CP00402C
42. Wei J, Chu X, Sun XY, *et al*. Machine learning in materials science. *InfoMat*. 2019;1(3):338-358.
doi: 10.1002/inf2.12028
43. Ng WL, Goh GL, Goh GD, Ten JS, Yeong WY. Progress and opportunities for machine learning in materials and processes of additive manufacturing. *Adv Mater*. 2024;36(34):e2310006.
doi: 10.1002/adma.202310006
44. Huang X, Ng WL, Yeong WY. Predicting the number of printed cells during inkjet-based bioprinting process based on droplet velocity profile using machine learning approaches. *J Intell Manuf*. 2023;35:2349-2364.
doi: 10.1007/s10845-023-02167-4
45. Shi J, Song J, Song B, Lu WF. Multi-objective optimization design through machine learning for drop-on-demand bioprinting. *Engineering*. 2019;5(3):586-593.
doi: 10.1016/j.eng.2018.12.009
46. Ning H, Zhou T, Joo SW. Machine learning boosts three-dimensional bioprinting. *Int J Bioprint*. 2023;9(4):739.
doi: 10.18063/ijb.739
47. Loessner D, Meinert C, Kaemmerer E, *et al*. Functionalization, preparation and use of cell-laden gelatin methacryloyl-based hydrogels as modular tissue culture platforms. *Nat Protoc*. 2016;11(4):727-746.
doi: 10.1038/nprot.2016.037
48. Ghosh RN, Thomas J, Vaidehi BR, *et al*. An insight into synthesis, properties and applications of gelatin methacryloyl hydrogel for 3D bioprinting. *Mater Adv*. 2023;4(22):5496-5529.
doi: 10.1039/D3MA00715D
49. Hogan NJ, Urban AS, Ayala-Orozco C, Pimpinelli A, Nordlander P, Halas NJ. Nanoparticles heat through light localization. *Nano Lett*. 2014;14(8):4640-4645.
doi: 10.1021/nl5016975
50. Pedregosa F, Varoquaux G, Gramfort A, *et al*. Scikit-learn: Machine learning in Python. *J Mach Learn Res*. 2011;12:2825-2830.
51. Smola AJ, Schölkopf B. A tutorial on support vector regression. *Stat Comput*. 2004;14(3):199-222.
doi: 10.1023/B:STCO.0000035301.49549.88
52. Breiman L. Random forests. *Mach Learn*. 2001;45(1):5-32.
doi: 10.1023/A:1010933404324
53. Singh AV, Bhardwaj P, Upadhyay AK, *et al*. Navigating regulatory challenges in molecularly tailored nanomedicine. *Explor Biomat X*. 2024;1(2):124-134.
doi: 10.37349/ebmx.2024.00009